Tunable photovoltaic effect and solar cell performance of self-doped perovskite SrTiO3

K. X. Jin, Y. F. Li, Z. L. Wang, H. Y. Peng, W. N. Lin et al.

Citation: AIP Advances **2**, 042131 (2012); doi: 10.1063/1.4766279

View online: http://dx.doi.org/10.1063/1.4766279

View Table of Contents: http://aipadvances.aip.org/resource/1/AAIDBI/v2/i4

Published by the American Institute of Physics.

Tunable photovoltaic effect and solar cell performance of self-doped perovskite $SrTiO_3$

K. X. Jin,[1] Y. F. Li,[1] Z. L. Wang,[1] H. Y. Peng,[1] W. N. Lin,[1] A. K. K. Kyaw,[2] Y. L. Jin,[3] K. J. Jin,[3] X. W. Sun,[2] C. Soci,[1] and Tom Wu[1,a]

[1]*Division of Physics and Applied Physics, School of Physical and Mathematical Sciences, Nanyang Technological University, 21 Nanyang Link, Singapore 637371, Singapore*

[2]*School of Electrical and Electronic Engineering, Nanyang Technological University, Singapore 639798, Singapore*

[3]*Beijing National Laboratory for Condensed Matter Physics, Institute of Physics, Chinese Academy of Sciences, Beijing 100190, P. R. China*

(Received 1 September 2012; accepted 23 October 2012; published online 2 November 2012)

We report on the tunable photovoltaic effect of self-doped single-crystal $SrTiO_3$ (STO), a prototypical perovskite-structured complex oxide, and evaluate its performance in Schottky junction solar cells. The photovaltaic characteristics of vacuum-reduced STO single crystals are dictated by a thin surface layer with electrons donated by oxygen vacancies. Under UV illumination, a photovoltage of 1.1 V is observed in the as-received STO single crystal, while the sample reduced at 750 °C presents the highest incident photon to carrier conversion efficiency. Furthermore, in the STO/Pt Schottky junction, a power conversion efficiency of 0.88% was achieved under standard AM 1.5 illumination at room temperature. This work establishes STO as a high-mobility photovoltaic semiconductor with potential of integration in self-powered oxide electronics. [http://dx.doi.org/10.1063/1.4766279]

In a typical bulk solar cell, a build-in field at the *p-n* or Schottky junction separates the photo excited electron-hole pairs, producing the photovoltage and the photocurrent.[1] Since it was introduced as the prime semiconductor in the 1950s, silicon has been the dominating material for constructing photovoltaic (PV) diodes and modules.[2] On the other hand, transition metal oxides (TMOs) are attractive choices for applications in energy-harvesting devices because most of them are abundant, cheap, and nontoxic. TMOs are also radiation-hard and chemically stable, thus their devices are suitable for being implemented in extreme environments. Besides, TMOs exhibit a wide range of fascinating electrical, magnetic and optical properties, promising for constructing multifunctional devices. Recently, there have been intensive efforts on incorporating ZnO and TiO_2, in particular their nanostructures, in dye-sensitized and polymer solar cells.[3–8] All-oxide solar cells were also fabricated based on *n*-type vertical zinc oxide nanowires and *p*-type cuprous oxide nanoparticles.[9] In terms of ternary perovskite oxides, ferroelectric PV effects in multiferroic $BiFeO_3$ (BFO) has drawn lots of attention recently.[10–12] Although the efficiency of BFO devices is very low, on the level of 0.01%, they exhibit interesting features such as polarization-dependent tunability and above-bandgap photovoltage.

As silicon is the basis of conventional electronic and photovoltaic applications, strontium titanate (STO) is the workhorse in the emerging technologies based on complex oxides.[13–15] Besides being a popular substrate for growing other perovskites,[16] STO exhibits rich and interesting physical properties. It is a quantum paraelectric material, but long-range ferroelectricity can be established in strained STO films.[17] Although the undoped STO is a transparent band insulator with a band gap of ~3.3 eV, electron doping can be achieved by either thermal reduction in vacuum or ion irradiation.

[a]Author to whom correspondence should be addressed; electronic-mail: tomwu@ntu.edu.sg.

These treatments generate high densities of oxygen vacancies, and these oxygen vacancies serve as singly ionized electron donors in STO single crystals;[18] thereby reduced STO shows *n*-type transport characteristics. In contrast to the extrinsic doping, the self-doping of oxygen vacancies does not introduce any chemical disorder. At relatively low carrier concentrations, STO shows insulator-to-metal transitions and even superconductivity.[19,20] Because of the large band gap of STO, most of the relevant optical studies have been carried out in the ultraviolet (UV) range. For example, undoped STO has been explored recently as the active material in UV photodetectors.[21,22] In addition, there have been studies on the UV-range PV effect in heterojunctions based on Nb-doped STO.[23,24] Very recently, more and more attention has been paid to the physical properties of reduced STO with tailored band structures. In a seminal work, Kan *et al.* reported blue light emission in Ar-irradiated and oxygen-deficient STO as a result of the formation of defect-related bands within the energy gap.[25,26] However, in spite of being one of the most prominent TMOs, STO has not been considered as an active material in bulk solar cells which need to operate in a broad range of wavelengths in the visible regime.

Here we systematically investigate the PV effect in STO/Pt Schottky junctions and examine the efficiency of a planar STO-based solar cell. Different reducing temperatures were used to systematically adjust the energy band structure of the STO, and defect-related bands are created within the bandgap. Under UV light illumination, a large photovoltage of ∼1.1 V was observed in the as-received STO single crystals, while the sample reduced at 750 °C presents the highest photocurrent thanks to the high mobility in semiconducting STO. For the self-doped STO devices with interdigitated electrodes, a power conversion efficiency of 0.88% was achieved under standard AM 1.5 solar illumination at room temperature. These results indicate that the STO junctions and their variants are promising for applications in energy-harvesting devices.

Commercial STO single crystals with a nominal (100) orientation purchased from CrysTec (Berlin) with dimension of $5\times5\times0.5$ mm^3 were reduced by thermal annealing in high vacuum (base pressure of $\sim10^{-6}$ mbar) at 550, 650, 750, and 850 °C for 30 minutes. The reduced samples are labeled as S55, S65, S75 and S85, respectively. UV-visible absorption spectra were measured on a Varian Cary 5000 spectrophotometer. Pt and Al/Pt electrodes were deposited sequentially through a shadow mask on STO by sputtering (the Pt overlayer on the Al electrode was used to prevent Al oxidation).

Transport measurements under monochromatic UV illumination were conducted using a UV light emitting diode with emission wavelength of 365 nm and power density of 2.6 W/cm^2. In the incident photon to carrier conversion efficiency (IPCE) measurements, the electrode dimension was 0.5 mm × 0.5 mm, and the distance between the two electrodes 0.5 mm. Measurements were carried out using the standard lock-in technique with a Xe lamp as the light source and a dispersion monochromator. The monochromatic light was modulated by a mechanical chopper at ∼140 Hz and focused onto the samples using a pair of parabolic mirrors. The collected data were normalized by the incident light intensity measured after each run with a calibrated Si photodiode. To simulate sunlight in power conversion efficiency (PCE) measurements we used an AM1.5 solar simulator (Model 16S-002, Solar Light Inc). The intensity of the incident beam is 100 mW/cm^2 as calibrated with a Thorlabs optical power meter before each measurement. To fabricate the solar cell device, interdigitated electrodes with a dimension of 20 μm × 100 μm were patterned on reduced STO substrates using photolithography. Cares were taken to ensure the maximum spatial uniformity of the light beam. A Keithley nano-voltmeter (model 2182A) was used to measure the photovoltage, and a multimeter (model 2635A) for current-voltage measurements.

The as-received STO single crystals are transparent and highly resistive, with resistance exceeding the limit of our measurement setup. By systematically increasing the reducing temperature while keeping the other conditions unchanged, we found that the sample resistance decrease significantly for temperature higher than ∼500 °C. The temperature-dependent sheet resistance data measured on four reduced samples are shown in Fig. 1(a). For a reducing temperature of 550 °C, the conduction of the STO single crystal remains semiconductor-like with thermally activated transport. However, when the reducing temperature increases to 650 °C, the sample starts showing metal-like behavior with decreased resistance on lowing measuring temperatures. Further increase of the reducing temperature to 750 and 850 °C results in a monotonous increase of conductivity. Using the

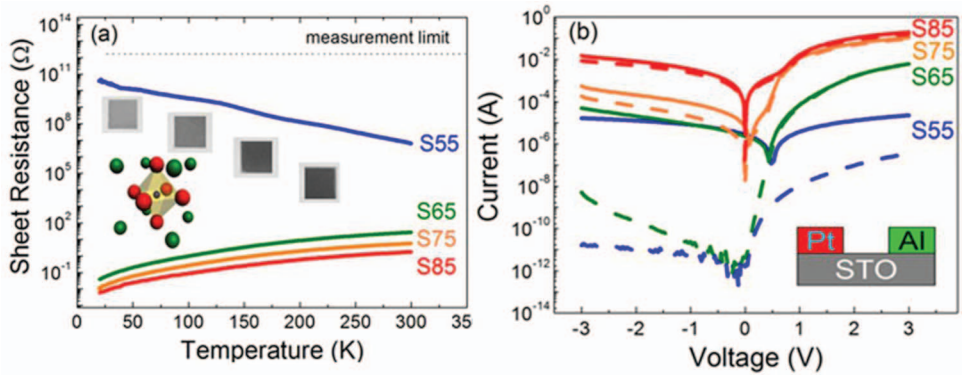

FIG. 1. (a) Temperature dependent sheet resistance data measured on STO single crystals annealed in vacuum at temperatures of 550 °C (S55), 650 °C (S65), 750 °C (S75), and 850 °C (S85). The resistance of the as-received STO substrate exceeds the measurement limit. The corresponding optical images of the reduced STO substrates are shown in the insets. Also illustrated is the atomic perovskite structure of STO, where the green, blue and red balls represent Sr, Ti and O atoms, respectively. (b) Semi-logarithmic plots of the room temperature current-voltage characteristics measured in various reduced STO samples both in the dark (dashed lines) and under UV light illumination. Inset shows the schematic of the Pt/STO/Al device.

Hall effect measurements, we determined the temperature-dependent carrier density of the 750 °C reduced sample. At 20 K, its sheet electron density is 1.2×10^{17} cm^{-2}, and the carrier mobility can be estimated as 5700 cm$^2 \cdot$ V$^{-1} \cdot$ s^{-1}, which is within the reported values measured on reduced STO single crystals. The reducing treatment is thus highly effective in tuning the electronic properties of STO; it is remarkable that the resistance can be modulated by more than seven orders of magnitude at room temperature and twelve orders of magnitude at 20 K.

It is noteworthy that the distribution of oxygen vacancies and the conduction in reduced bulk STO single crystals are quite inhomogeneous due to the small diffusion coefficient of oxygen ions in STO. This has been noted in a few previous studies on reduced STO single crystals.[27–29] If we assume a diffusion constant D of about 10^{-9} cm^2/s at the annealing temperature and the annealing time t of 30 minutes, the diffusion length $l = \sqrt{D \cdot t}$ of oxygen ions can be calculated to be about 13.4 μm, which can then be taken as the thickness of the oxygen-vacancy-rich surface layer. It is noteworthy that a higher annealing temperature corresponds to a larger diffusion constant, leading to a thicker reduced layer containing a higher number of oxygen vacancies. While these oxygen vacancies serve as electron donors in the reduced surface layer, the bulk single crystal underneath remains undoped and highly insulating. Although prolonging the reduction time may increase thickness and improve homogeneity of the self-doped layer, the self-healing effect during long reducing processes can substantially decrease the density of initially introduced vacancy defects and even destroy the metallic state;[29] thus, we fixed the annealing time in our experiments at 30 minutes. For proper interpretation of the data, it is important to keep in mind that for all the annealing conditions used in this work, the highly reduced conducting surface layer is much thinner than the bulk single crystal which has a thickness of 0.5 mm.

The optical images of the STO single crystals reduced at different temperatures are shown in the inset of Fig. 1(a). The introduction of oxygen vacancies turns STO from a transparent insulator into opaque semiconductors/metals, and the color progressively deepens as the reducing temperature increases. Both the insulator-to-metal transition and the change of optical properties can be attributed to the emergence of a metallic defect-related subband structure in the reduced STO surface layers. This result is consistent with the results of previous photoluminescence studies on reduced STO single crystals.[25,26]

Fig. 1(b) shows the room temperature current-voltage characteristics of the reduced STO single crystals in the dark (dashed curves) and under UV illumination (solid curves). The schematic of the electrode configuration used for these measurements is illustrated in the inset, where Pt and Al were selected as the electrode materials. Because of the wide usage of STO and the ubiquitous presence of metal electrodes, the physical properties of metal/STO heterojunctions have been well

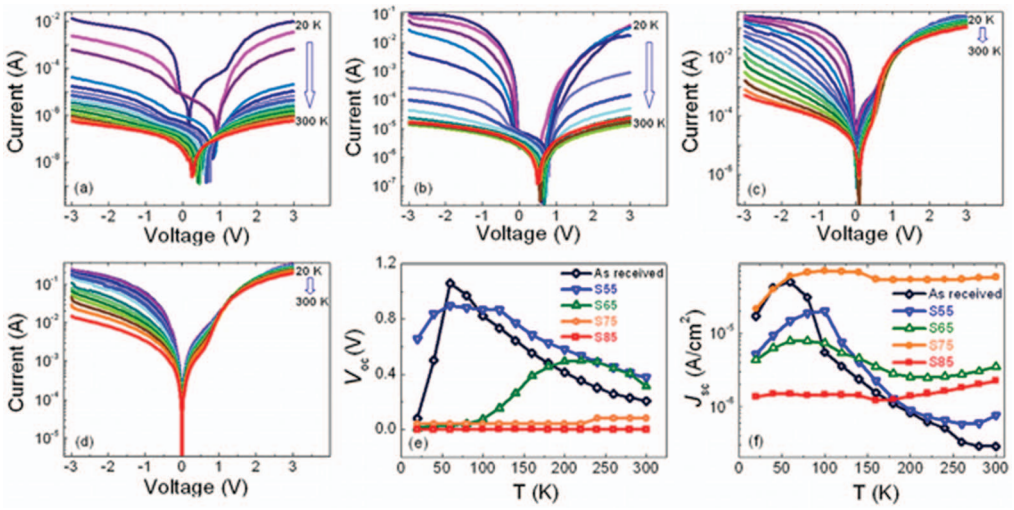

FIG. 2. Typical current-voltage curves measured at various temperatures (from 20 K to 300 K with a 20 K interval) under UV illumination in junctions made of (a) as-received STO single crystal, (b) S55 sample, (c) S75 sample and (d) S85 sample. The open-circuit voltage V_{OC} (e) and the short-circuit current density J_{SC} (f) as a function of the measurement temperature for junctions based on various reduced STO single crystals.

explored.[30–33] In general, without the significant pinning of Fermi level, the barrier height at the interface is related to the work function of the metal used. In our heterojunctions, the Al/STO interface shows an ohmic behavior, whereas Pt is expected to form a Schottky junction with STO as it has one of the highest work functions among all metal. In the measurements the positive bias is defined as the current flowing from the Pt electrode into the STO single crystals, and it is also the forward bias direction. At room temperature and in the dark, the current-voltage curves of these Schottky junctions show good rectifying characteristics. The room temperature rectification ratios at 3 V are 2.3×10^4, 1.1×10^6, 5.1×10^2 and 12.6 for the S55, S65, S75 and S85 samples, respectively. Overall, the rectification ratio is highest for the sample reduced at 650 °C, and it decreases for higher reducing temperatures.

The current-voltage curves of the samples were also measured under UV illumination with photon energy ($\lambda = 365$ nm, $E_{ph} \sim 3.4$ eV) slightly above the STO band gap (~3.3 eV). Given the absorption coefficient (α) of STO in this spectral range,[34] full absorption is expected since the penetration depth which is approximately given by $1/\alpha \sim 7$ μm is much smaller than the thickness of the STO substrate (0.5 mm). The UV light irradiation significantly increases the junction current; as a result, the room temperature rectification ratios at 3 V decrease to 0.7, 118.7, 201.1 and 12.5 for the S55, S65, S75 and S85 samples, respectively. The effect of light illumination is negligible in S85 because in this highly reduced sample the concentration of intrinsic carriers is already very high and the photo-excited carriers do not cause a significant effect.

Fig. 2(a)–2(d) show the typical temperature-dependent current-voltage characteristics of the as-received and the annealed STO single crystal samples measured under the UV light illumination. The as-received STO is very insulating and displays significant photoconductivity upon UV light irradiation. The large shifts of open-circuit voltage (V_{OC}) indicate the appearance of notable photovoltage. In general, the photocurrent appears to be higher in the reduced samples, but the photovoltage is smaller compared to the as-received single crystal.

V_{OC} and the short-circuit current density (J_{SC}) of the as-received and the reduced STO single-crystal samples as a function of the measuring temperatures are summarized in Fig. 2(e) and 2(f), respectively. The highest V_{OC} of about 1.1 V occurs in the as-received STO single crystal at 60 K, while S55 presents the highest photovoltage at room temperature of about 0.37 V. For S85, the photovoltage remains very low in the whole temperature range. On the other hand, J_{SC} exhibits a maximum value of about 7×10^{-2} mA/cm^2 at 100 K in S75, and remains roughly constant up to room temperature. In general, J_{SC} of the samples increases as the measurement temperature decreases from

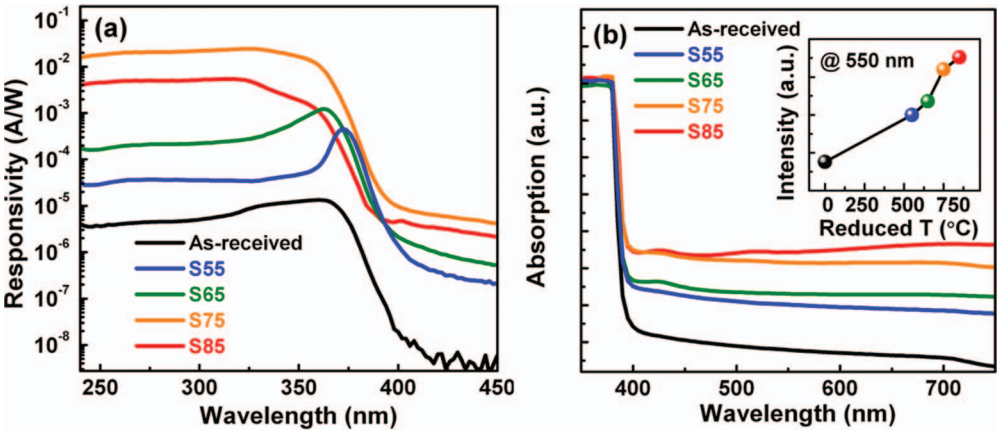

FIG. 3. (a) Incident photon to charge carrier conversion efficiency (IPCE) spectra measured in the Pt/STO/Al devices made of the as-received and the reduced STO single crystals. (b) Optical absorption spectra of the samples. The inset highlights the significant enhancement of absorption intensity in the visible region (at 550 nm) as the reducing temperature increases.

room temperature, which is a result of the enhanced mobility at low temperatures in oxygen-reduced STO.[27] On cooling down, J_{SC} diminishes at the low temperatures, i.e., below ~100 K, due to the weakened thermal activation of carriers.

Fig. 3(a) shows the IPCE (i.e. the number of charge carriers collected per incident photon) spectra for the reduced samples and the as-received STO single crystal. In the as-received STO, the photoresponsivity is very low in the visible range, but it increases significantly for wavelengths smaller than ~400 nm. The maximum IPCE occurs at 360 nm, which almost coincides with the band gap energy of STO, suggesting that the main photo-excitation mechanism is associated with the interband transitions. Compared to the as-received STO single crystals, the reducing treatment significantly increases the photoresponsivity in both the UV and the visible spectral ranges. The sample S75 which is reduced at 750 °C exhibits the highest IPCE, and the improvement throughout the wavelength range is more than three orders of magnitude. The increase of photoresponsivity must be related to the conducting surface layer upon annealing because the optical property of the undoped portion of the STO single crystal remains the same. The overall IPCE spectra are still dominated by the UV response because the undoped portion of the single-crystal substrate is much thicker than the doped surface layer. On the other hand, the highly conducting surface layer serves as an effective channel with high mobility for the flow of photocurrent; as a result, even the UV responsivity is improved in the reduced samples.

In order to investigate the application of the Pt/STO/Al Schottky junctions in solar cells, we examined the UV-visible absorption of the various STO samples. As shown in Fig. 3(b), sharp absorption edges are located at ~385 nm, corresponding to the band gap of STO. This is in agreement with the data in Fig. 3(a) and similarly can be attributed to the dominating absorption of the undoped bulk. On the other hand, thanks to the reduced surface layer, the reducing treatments significantly enhance light absorption in the visible region below the band gap. The absorbance at 550 nm monotonously increases with the reducing temperature, as shown in the inset of Fig. 3(b). This is also consistent with the darker hue observed in STO single crystals reduced at higher temperatures (shown in the inset of Fig. 1(a)).

In order to understand the photoconductive properties of the Pt/STO devices, we calculated the energy band alignment at the metal-semiconductor junction by solving the Poisson's equation and the Boltzmann equation self-consistently.[35,36] The schematic of the energy band of the junction is illustrated in Fig. 4(a). When STO is brought in contact with Pt, charge transfer between the large metal Fermi surface of Pt and the various valley points of the STO conduction band restores the electrostatic equilibrium and induces alignment of the Fermi levels. During this process, a space charge region accompanied by a built-in field is formed at the junction interface. The work function of Pt is about 5.5 eV, and the electron affinity of STO is assumed to be about 4.2 eV.[37] The Fermi

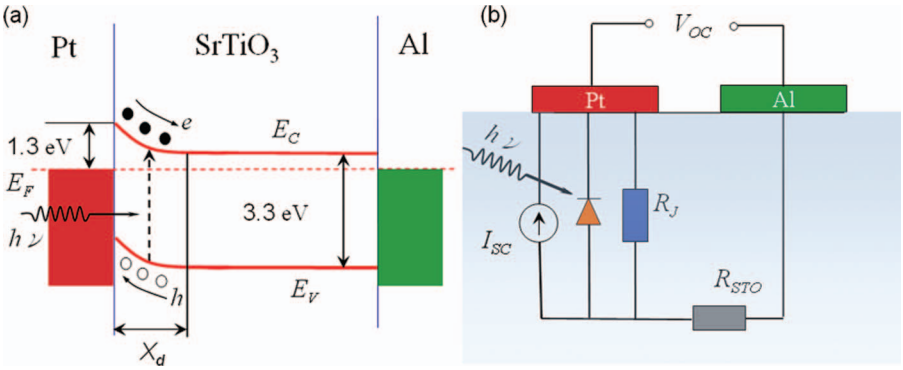

FIG. 4. (a) Schematic band structure of the Pt/STO/Al heterojunction. The PV effect occurs when the junction is irradiated by the light and the photo-excited electron/hole pairs are separated by the build-in field in the depletion layer. (b) Equivalent circuit which models the photoelectronic measurement processes in the junction.

level of STO can be calculated using the formula:

$$E_{fs} = E_c + k_0 T \ln(\frac{N_d}{N_c}), \tag{1}$$

where E_c is the energy of the conduction band edge, T is the temperature which was taken as 300 K in our calculation, k_0 is the Boltzmann constant, N_d is the ionized donor density, and N_c is the effective density of states in the conduction band. If we assume a typical donor density of 10^{19} cm^{-3}, the resulting Fermi level is 0.07 eV below the conduction band edge. The thickness of the depletion layer denotedas X_d in Fig. 4(a) is calculated to be ~80 nm by solving Poisson and Boltzmann equations self-consistently.[35,36] Upon irradiation, electron-hole pairs are generated and separated by the build-in field in the depletion layer, generating the photocurrent. An additional advantage of using STO single crystals in PV devices is the high dielectric constant ($\varepsilon_r \sim 300$ at room temperature, and it can reach 10^4 at low temperatures).[38] Such a high dielectric constant not only facilitates the formation of the depletion layer and the photogeneration of electron-hole pairs, but also reduces carrier scattering by screening charged defects, overall enhancing the PV efficiency.

The correlation between the electronic properties of the Pt/STO/Al junctions and the PV effect can be understood using the equivalent circuit in Fig. 4(b). An equivalent DC current source provides the photocurrent and is connected in parallel with a Schottky diode and a shunt resistance (R_J). The R_J takes into account the loss of carriers via various leakage pathways. Another key component of the circuit is a series resistor (R_{STO}) which accounts for the bulk resistance of the STO single crystal, the contact resistance between STO and the Al electrode, and the parasitic resistance associated with the interconnections. The as-received STO single crystal is a prototypical insulator, and the large R_{STO} leads to the very small photocurrent observed at room temperature (Fig. 2(d)). On the other hand, the highly reduced STO sample, in particular S85, is very leaky, and the very small R_J leads to negligible photovoltage. Thus, it is of paramount importance to optimize both resistive components to achieve the optimal performance.

To the best of our knowledge, although STO is a prototypical perovskite oxide, there has been no report on evaluating the performance of STO-based solar cells under the illumination of visible light. In our experiments to incorporate self-doped STO single crystals in solar cells, we used the sample S75 to construct solar cell devices because it exhibits the highest IPCE. Fig. 5 shows the current-voltage characteristic of the STO-based solar cell in dark and under simulated AM 1.5 illumination, where interdigitated electrodes were patterned using photolithography to increase the active junction area of the device. The inset of Fig. 5 shows the scanning electron microscopy image of the device with semitransparent (~15 nm thick) interdigitated Pt electrodes. The resulting open-circuit voltage V_{OC} of the junction solar cell is about 0.1 V. The rather low V_{OC} may be attributed to the recombination of electrons at anode and the reduced junction resistance, as follows from the

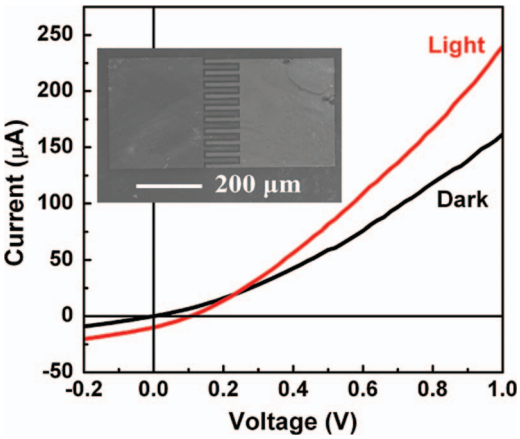

FIG. 5. Current-voltage curves of the Pt/STO/Al Schottky junction made of the S75 sample measured either in dark and under the illumination of a simulated solar light AM 1.5 (100 mW/cm^2). The inset shows a scanning electron microscopy image of the device with interdigitated semitransparent Pt (left) and Al (right) electrodes.

general expression of V_{OC}:

$$V_{OC} = \frac{nkT}{q} \ln\left(\frac{J_{SC}}{J_0}\right), \tag{2}$$

where n is the ideality factor, k is the Boltzmann constant, T is the temperature, q is the elemental electron charge, J_{SC} is the short-circuit current density, and J_0 is the saturation current density. Eq. (2) shows the importance of reducing J_0 and increasing J_{SC} by reducing any undesired carrier recombination to increase the open circuit voltage. Alternatively, other strategies such as imposing virtual contacts could also be implemented to induce photovoltage multiplication.[39]

Remarkably, the short-circuit current of the device is of the order of 10 mA. If we only consider the active area delimited by the interdigitated electrodes, i.e. 100 μm × 300 μm, this corresponds to a current per illuminated area of ~35 mA/cm^2. This value is consistent with the short circuit-current density that can be calculated from the IPCE spectra using the formula:

$$J_{SC} = \int qG(\lambda)IPCE(\lambda)d\lambda, \tag{3}$$

where $G(\lambda)$ is the standard AM1.5 solar photon flux at wavelength λ. However, due to the particular surface configuration employed in this device, the photocurrent per illuminated area does not correspond to the photocurrent density of conventional thin-film solar cells in the sandwich-type configuration.

The key performance metric of a solar cell is the power conversion efficiency (PCE), which is defined as:

$$\eta = (I_M \times V_M)/P_{in} = (FF \times I_{sc} \times V_{oc})/P_{in}, \tag{4}$$

where I_M and V_M describe the bias point where the photo-generated power reaches the maximum, P_{in} is the power density of the incident light and FF is the fill factor. The PCE of the STO-based junction in Fig. 5 is about 0.88%, and its FF is 0.25. These values are much higher than those obtained so far in junctions based on similar perovskite oxides, such as BFO.[10–12] Further improvement of the power conversion efficiency could be achieved by increasing the optical absorption in the visible range, for instance by making use nanoscale surface engineering for light trapping[40–42] or other strategies like plasmonics enhancement.[43]

In summary, the PV performance of Schottky heterojunctions based on self-doped STO single crystals was systematically investigated. Reduction of the STO crystals by thermal annealing can be effectively used to tailor the electronic structure of pristine insulating STO by introducing oxygen vacancies within a self-doped surface layer. This simple approach can effectively extend the optical

absorption of STO into the visible spectral range and improves the charge transport properties. The STO/Pt heterojunctions exhibit rectifying behaviors which can be readily tuned by the reducing temperature and by the light illumination. A V_{OC} of about 1.1 V was observed under UV illumination in the as-received STO single crystal, whereas the oxygen-reduced samples exhibit tunable optical absorption and higher IPCE. Furthermore, a power conversion efficiency of 0.88% was obtained under standard solar illumination in the STO single crystal reduced at 750 °C. We believe that a higher efficiency may be achieved in STO-based solar cells by adopting different device structures, for example using the sandwich geometry to suppress the series resistance. Complementary to the existing works in literature, our results underline STO as a versatile perovskite TMO, and this work provides an example of its potential in energy conversion applications. Hopefully the data presented herein will stimulate intensive future endeavors to cultivate the viability of functional perovskite oxides as active materials for energy-harvesting technologies.

ACKNOWLEDGMENTS

We acknowledge the support from the National Research Foundation of Singapore. This work is also supported in part by the National Natural Science Foundation of China (NSFC) (Project Nos. 61006037, 61076015 and 51172183).

[1] J. Nelson, *The physics of solar cells* (Imperial College press, London, 2003).
[2] A. Shah, P. Torres, R. Tscharner, N. Wyrsch, and H. Keppner, Science **285**, 692 (1999).
[3] B. O'Regan and M. Graezel, Nature **353**, 737 (1991).
[4] U. Bach, D. Lupo, P. Comte, J. E. Moser, F. Weissörtel, J. Salbeck, H. Spreitzer, and M. Grätzel, Nature **395**, 583 (1998).
[5] M. Law, L. E. Greene, J. C. Johnson, R. Saykally, and P. Yang, Nat. Mater. **4**, 455 (2005).
[6] A. K. K. Kyaw, X. W. Sun, J. L. Zhao, J. X. Wang, D. W. Zhao, X. F. Wei, X. W. Liu, H. V. Demir, and T. Wu, J. Phys. D - Appl. Phys. **44**, 045102 (2011).
[7] A. K. K. Kyaw, H. Tantang, Q. Zhang, T. Wu, L. Ke, C. Peh, Z. H. Huang, X. T. Zeng, H. V. Demir, and X. W. Sun, Appl. Phys. Lett. **99**, 021107 (2011).
[8] A. K. K. Kyaw, H. Tantang, T. Wu, L. Ke, J. Wei, H. V. Demir, Q. C. Zhang, and X. W. Sun, J. Phys. D - Appl. Phys. **45**, 165103 (2012).
[9] B. D. Yuhas and P. Yang, J. Am. Chem. Soc. **131**, 3756 (2009).
[10] T. Choi, S. Lee, Y. J. Choi, V. Kiryukhin, and S.-W. Cheong, Science **324**, 63 (2009).
[11] W. Ji, K. Yao, and Y. C. Liang, Adv. Mater. **22**, 1763 (2010).
[12] S. Y. Yang, J. Seidel, S. J. Byrnes, P. Shafer, C.-H. Yang, M. D. Rossell, P. Yu, Y.-H. Chu, J. F. Scott, J. W. Ager, III, L. W. Martin, and R. Ramesh, Nat. Nanotechnol. **5**, 143 (2010).
[13] A. P. Ramirez, Science **315**, 1377 (2007).
[14] H. Chen, A. M. Kolpak, and S. Ismail-Beigi, Adv. Mater. **22**, 2881 (2010).
[15] D. G. Schlom and J. Mannhart, Nat. Mater. **10**, 168 (2011).
[16] M. Kawasaki, K. Takahashi, T. Maeda, R. Tsuchiya, M. Shinohara, O. Ishiyama, T. Yonezawa, M. Yoshimoto, and H. Koinuma, Science **266**, 1540 (1994).
[17] J. H. Haeni, P. Irvin, W. Chang, R. Uecker, P. Reiche, Y. L. Li, S. Choudhury, W. Tian, M. E. Hawley, B. Craigo, A. K. Tagantsev, X. Q. Pan, S. K. Streiffer, L. Q. Chen, S. W. Kirchoefer, J. Levy, and D. G. Schlom, Nature **430**, 758 (2004).
[18] R. Moos, W. Mcnesklou, and K. H. Hairdtl, Appl. Phys. A. **61**, 389 (1995).
[19] J. F. Schooley, W. R. Hosier, E. Ambler, and J. H. Becker, Phys. Rev. Lett. **14**, 305 (1965).
[20] K. Ueno, S. Nakamura, H. Shimotani, A. Ohtomo, N. Kimura, T. Nojima, H. Aoki, Y. Iwasa, and M. Kawasaki, Nat. Mater. **7**, 855 (2008).
[21] J. Xing, K. Zhao, H. B. Lu, X. Wang, G. Z. Liu, K. J. Jin, M. He, C. C. Wang, and G. Z. Yang, Opt. Lett. **32**, 2526 (2007).
[22] E.-J. Guo, H.-B. Lu, M. He, J. Xing, K.-J. Jin, and G.-Z. Yang, Appl. Opt. **49**, 2557 (2010).
[23] Y. Muraoka, T. Muramatsu, J. Yamaura, and Z. Hiroi, Appl. Phys. Lett. **85**, 2950 (2004).
[24] T. Muramatsu, Y. Muraoka, and Z. Hiroi, Jpn. J. Appl. Phys. **44**, 7367 (2005).
[25] D. Kan, T. Terashima, R. Kanda, A. Masuno, K. Tanaka, S. Chu, H. Kan, A. Ishizumi, Y. Kanemitsu, Y. Shimakawa, and M. Takano, Nat. Mater. **4**, 816 (2005).
[26] D. Kan, R. Kanda, Y. Kanemitsu, Y. Shimakawa, and M. Takano, T. Terashima, and A. Ishizumi, Appl. Phys. Lett. **88**, 191916 (2006).
[27] Q. N. Tufte and P. W. Chapman, Phys. Rev. **155**, 796 (1967).
[28] H. P. R. Frederikse, W. R. Hosler, W. R. Thurber, J. Babiskin, and P. G. Siebenmann, Phys. Rev. **158**, 775 (1967).
[29] K. Szot, W. Speier, R. Carius, U. Zastrow, and W. Beyer, Phys. Rev. Lett. **88**, 075508 (2002).
[30] R. C. Neville and C. A. Mead, J. Appl. Phys. **43**, 4657 (1972).
[31] T. Shimizu and H. Okushi, J. Appl. Phys. **85**, 7244 (1999).
[32] T. Susaki, Y. Kozuka, Y. Tateyama, and H. Y. Hwang, Phys. Rev. B **76**, 155110 (2007).
[33] M. Mrovec, J.-M. Albina, B. Meyer, and C. Elsässer, Phys. Rev. B **79**, 245121 (2009).
[34] M. Capizzi and A. Frova, Phys. Rev. Lett. **25**, 1298 (1970).
[35] K. J. Jin, H. B. Lu, Q. L. Zhou, K. Zhao, B. L. Cheng, Z. H. Chen, Y. L. Zhou, and G. Z. Yang, Phys. Rev. B **71**, 184428 (2005).

[36] Q. L. Zhou, K. J. Jin, H. B. Lu, P. Han, Z. H. Chen, K. Zhao, Y. L. Zhou, and G. Z. Yang, Europhys. Lett. **71**, 283 (2005).
[37] Y. W. Chung and W. B. Weissbard, Phys. Rev. B **20**, 3456 (1979).
[38] T. Sakudo and H. Unoki, Phys. Rev. Lett. **26**, 851 (1971).
[39] L. Yang, S. Wang, Q. Zeng, Z. Zhang, T. Pei, Y. Li, and L. M. Peng, Nat. Photonics **5**, 672 (2011).
[40] M. D. Kelzenberg, S. W. Boettcher, J. A. Petykiewicz, D. B. Turner-Evans, M. C. Putnam, E. L. Warren, J. M. Spurgeon, R. M. Briggs, N. S. Lewis, and H. A. Atwater, Nat. Mater. **9**, 239 (2010).
[41] X. Sheng, J. Liu, I. Kozinsky, A. M. Agarwal, J. Michel, and L. C. Kimerling, Adv. Mater. **23**, 843 (2011).
[42] C. Battaglia, J. Escarré, K. Söderström, M. Charrière, M. Despeisse, F. Haug, and C. Ballif, Nat. Photonics **5**, 535 (2011).
[43] H. A. Atwater and A. Polman, Nat. Mater. **9**, 205 (2010).